Effect of Bumpy Magnetic Field on Energy Confinement in NBI Plasmas of Heliotron J

S. Kobayashi 1), T. Mizuuchi 1), K. Nagasaki 1), H. Okada 1), K. Kondo 2), S. Yamamoto 1), S. Murakami 3), D. Katayama 2), Y. Suzuki 4), T. Minami 4), K. Nagaoka 4), Y. Takeiri 4), K. Murai 2), Y. Nakamura 2), M. Yokoyama 4), K. Hanatani 1), G. Motojima 4), K. Hosaka 2), K. Toushi 1), F. Sano 1)

1) Institute of Advanced Energy, Kyoto University, Gokasho, Uji 611-0011, Japan
2) Graduate School of Energy Science, Kyoto University, Gokasho, Uji 611-0011, Japan
3) Graduate School of Engineering, Kyoto University, Kyoto 606-8501, Japan
4) National Institute for Fusion Science, Toki, Gifu, 509-5292, Japan

e-mail: kobayashi@iae.kyoto-u.ac.jp

Abstract. The energy confinement in the NBI plasmas has been investigated in the helical-axis heliotron device, Heliotron J. The configuration control experiments for bumpiness (ε_b), being one of the side-bands of the helical component, show that the plasma performance in NBI plasmas depends on not only the effective helical ripple (ε_{eff}) but also the bumpiness. The preferable enhancement factor of the experimental energy confinement time to the international stellarator scaling law ISS95 has been obtained in the high-ε_b configuration and in the low-ε_{eff} (i.e. medium-ε_b) condition. The improvement in the ion and electron temperature contributes to the enhancement of the plasma performance in the high-ε_b configurations since the fast ion confinement is found to be better in this configuration. The control of bumpiness is effective not only in the energetic particle transport but also in the global energy confinement in NBI plasmas of Heliotron J.

1. Introduction

For the optimization of helical/stellarator magnetic configurations toward the fusion reactor, it is important how to reduce the ripple loss of helically trapped particle and to control the neoclassical transport since the magnetic field has the three-dimensional structure. Some optimization studies for advanced stellarator configurations have been done from the point of view to obtain the symmetry of the magnetic field (quasi-symmetry concept) [1,2] and adjusting the Fourier harmonics of the confinement field to appropriate values. In the planner axis heliotron configurations such as LHD, Heliotron E and CHS [3-5], confinement of the high energy particles has been improved when the magnetic axis is shifted inwardly since the drift orbit surface is optimized (drift optimization). In the Boozer coordinate system, side-band of the helical magnetic field is adjusted in the inward-shifted configuration, which plays a role to reduce the loss of trapped particles. In such case, reduction in neoclassical transport coefficient in the $1/\nu$ regime has also been found [6], and furthermore, the experimentally obtained energy confinement time has been found to be better than that of the outward shifted configurations [7,8]. These results suggest that the drift optimization is considered to be one of the candidates to mitigate the anomalous transport.

The Heliotron J device [9,10] is a medium sized helical-axis heliotron device with an L/M=1/4 helical coil to explore the concept of optimization of the helical-axis heliotron concept which is based on the omnigeneous optimization scenario [11,12]. In the helical-axis heliotron configuration, the theoretical analysis has predicted that the control of the toroidal mirror ratio, bumpiness, in the Boozer coordinate system is important to control the ripple loss of trapped particle and the neoclassical transport, since it has been found that the neoclassical diffusion coefficient or the loss rate of the energetic particles have a dependence on bumpiness. Note that one of the features of the Heliotron J configuration is that the

The final version of this paper will be presented in IAEA website,
http://www-pub.iaea.org/MTCD/Meetings/Announcements.asp?ConfID=165

strength of the bumpiness can vary with keeping a magnetic well in the whole plasma region inside the last closed flux surface (LCFS) and without the change of the magnetic axis position.

The previous experimental study on the high energy ion transport revealed that the control of bumpiness has been effective to the energetic ion confinement, that is, the 1/e decay time of the high energy CX flux after turning-off of NBI becomes longer as increasing the strength of bumpiness [13]. However, the global energy confinement in the NBI heated plasmas and its bumpiness effect have not been investigated systematically. In this paper, we study the global energy confinement in the NBI plasmas of Heliotron J, focusing on the bumpiness effect on the confinement. We carried out the bumpiness scan experiment in the NBI plasmas. The energy confinement is investigated by changing the NBI injection power at the same density condition.

2. Experimental setup

2.1. Heliotron J device

Figure 1 shows the bird's-eye view of Heliotron J including the coils and the heating systems. To achieve a flexible configuration control in Heliotron J, five sets of coils are installed, i.e. helical and main vertical (H+V), toroidal A and B (TA and TB) and inner and auxiliary vertical (IV and AV) coils. The TA coils are located at so-called "corner" section where tokamak like magnetic field is formed. On the contrary, the magnetic field in the "straight" section in which the TB coils are set has a local quasi-omnigeneous magnetic field. As shown in Fig. 1, two tangential beamlines of the hydrogen neutral beam injection (NBI) system has been installed in Heliotron J (BL1 and BL2). Each beamline has two bucket-type ion sources and the maximum beam power and acceleration voltage of 0.7 MW and 30 keV, respectively. The mean pitch angle of the beam ions is about 155 (25) degree in the co- (counter-) injection case of the standard configuration of Heliotron J. The numerical analysis of the NBI absorption power is described in section 3 in detail. An E//B type CX-NPA system can measure the hydrogen and deuterium neutral fluxes separately. This system also has a capability to scan both poloidal (θ_{NPA}) and toroidal (ϕ_{NPA}) angles with the ranges of $-3^{o} < \theta_{NPA} < +10^{o}$ and $-10^{o} < \phi_{NPA} < +18^{o}$. The initial plasma is produced by 2nd harmonic 70 GHz ECH with a maximum injection power of 0.4 MW. The deuterium gas was used for working gas to obtain the energy spectra for bulk (D^{+}) and beam (H^{+}) ions separately.

2.2. Configuration characteristics of bumpiness scan experiment

In this study, we selected three bumpiness ε_b (= B_{04}/B_{00}) configurations of high (ε_b = 0.15), medium (0.06) and low (0.02) at r/a = 2/3 by changing the current ratio of TA and TB coils with almost keeping the edge rotational transform ($\iota(a)/2\pi$ = 0.56), plasma volume (V_p = 0.7 m^3), and magnetic axis position (R_{ax} = 1.2 m) constant. Figures 2(a)-(c) show the radial profiles of the bumpiness, helicity ε_t (= B_{14}/B_{00}) and toroidicity ε_t (= B_{10}/B_{00}), where B_{mn} is the Fourier component of the

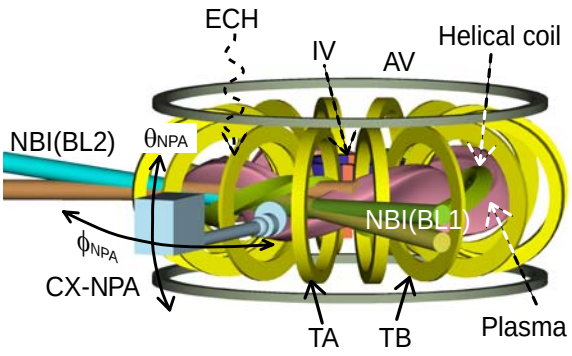

Fig. 1. Schematic view of Heliotron J including coil, heating and diagnostic systems.

field strength with m/n mode numbers in the Boozer coordinate system. The standard configuration of Heliotron J corresponds to medium-ε_b configuration. In the low-ε_b configuration the bumpiness can change its sign in the core region. As shown in Figs. 2(a)-(c), other main Fourier components, i.e. helicity and toroidicity, are almost unchanged to clarify the bumpiness effect on the energy confinement. Figures 2(d)-(f) illustrates the magnetic field strength at r/a = 0.4 along a field line in the Boozer coordinate system. In the case of high-ε_b, the ripple amplitude is higher than the others and the minimum values of field strength at the bottoms of the ripple are relatively flat. In contrast, in the configuration with low-ε_b, the strength of the ripple bottoms varies along the field line. From the viewpoint of the Boozer coordinate system, it has been found that the difference between $\boldsymbol{B}$ and $\nabla\boldsymbol{B}$ becomes small as increasing bumpiness, which expects the reduction in the gap between drift and flux surfaces in the high-ε_b configuration.

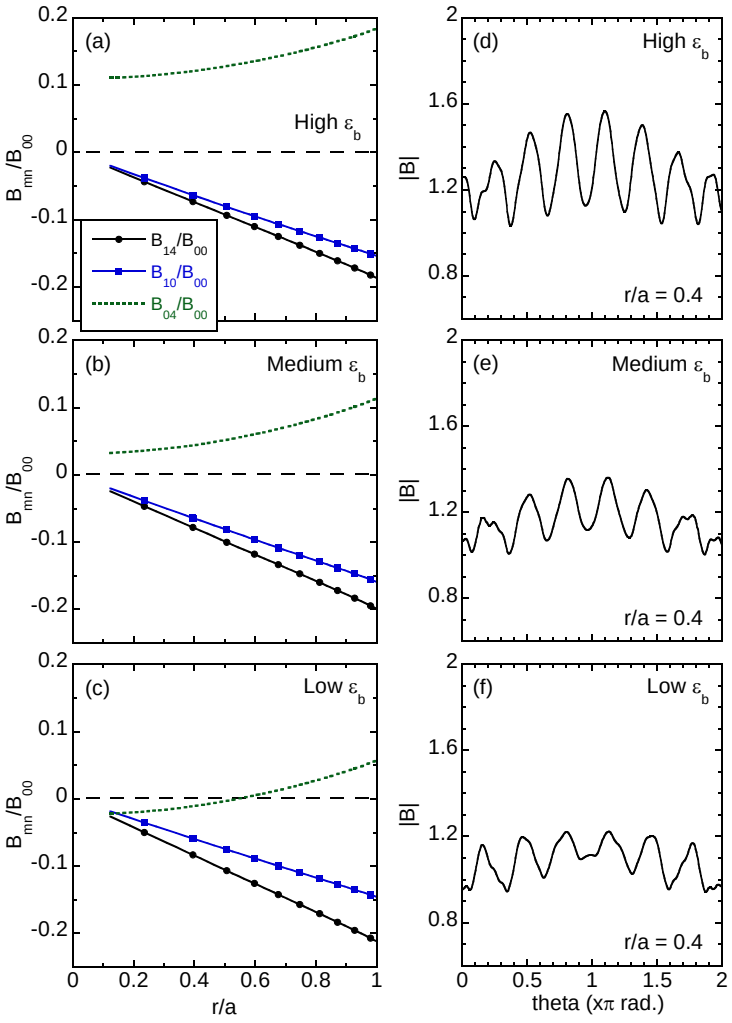

Fig. 2. (a)-(c) Radial profile of, helicity, toroidicity and bumpiness in Boozer coordinate systems and (d)-(f) field strength along the field line in the high-, medium and low-ε_b configurations.

The effective helical ripple ε_{eff} is one of the indexes of the neoclassical transport coefficient in the $1/\nu$ regime since the neoclassical diffusion coefficient D is proportional to $\varepsilon_{eff}^{2/3} \cdot \nu_d^2 / \nu$, where ν_d and ν are the drift velocity and the collisionality, respectively [14]. The effective helical ripple at r/a = 2/3 estimated by Monte-Carlo technique with DCOM [15] is 0.22, 0.13 and 0.26 for the high-, medium- and low-ε_b configurations, respectively, that is, medium-ε_b has the lowest ε_{eff} among the three configurations.

3. Power absorption analysis for NBI

Prior to the experiment, the beam absorption profile was estimated by the following three steps [16]; (1) calculation of birthpoints of the beam ions using Monte-Carlo method (HFREYA), (2) estimation of orbit loss and the redistribution of the beam ions by orbit calculation for ion guiding center (MCNBI) and (3) analysis of heating profile using Fokker-Planck equation (FIT) [17]. The Monte-Carlo code HFREYA is modified to apply the three-dimensional shape of the plasma and the inner vacuum vessel of Heliotron J. The ion orbit is

calculated at the initial energy of beam ions without slowing down process, that is, we do not treat the orbit loss of fast ions including the slowing down processes in this calculation. The slowing down process of fast ions and the energy transfer to both the bulk electrons and ions are calculated by the Fokker-Planck analysis including the CX loss of fast ions.

Figure 3(a) shows the radial profile of the beam absorption under the line-averaged electron density ($\bar{n}_e$) from 1×10^{19} to 3×10^{19} m^{-3} in the medium-ε_b (standard) configuration in the counter NBI case. The density profiles were assumed to be parabolic one. The radial profile of the electron (ion) temperature also has parabolic one with the core temperature of 400 eV (300 eV). The neutral beam is deposited around the core region and the shape of the absorption profile is similar to each other under the density range. Therefore, the experiments can be carried out with keeping the heating deposition profile almost unchanged. Figure 3(b) shows the total beam absorption rate as a function of the line-averaged electron density in the high, medium and low-ε_b configurations. The absorption rate in the three configurations increases from 0.2 to 0.4 as increasing the density. The configuration dependence is not so clear under the condition.

4. Results and discussions

Figure 4 shows the plasma stored energy as a function of the absorbed NBI power (P_{abs}) in the three bumpiness configurations. These data were obtained at the averaged electron density of 2×10^{19} m^{-3} in the counter injected neutral beam plasmas. The stored energy is evaluated by the diamagnetic loop data. The stored energy in the high- and medium-ε_b configurations is clearly higher than that in the low ε_b case. The difference of W_{dia} between the high- and medium-ε_b configurations is small, but the W_{dia} in high-ε_b case is more than 5% higher than that of the medium-ε_b configuration.

Figure 5(a) shows the bulk (deuterium) ion temperature deduced by CX-NPA as a function of the NBI absorption power P_{abs} obtained in the three ε_b configurations. An increase in the ion temperature as increasing ε_b is observed, that is, the ion temperature in the high, medium- and low-ε_b configurations are 0.23, 0.20 and 0.18 keV at P_{abs} of 200 kW, respectively. As shown in Fig. 5(b), the electron cyclotron emission intensity (I_{ECE}) at the core region increased with P_{abs} in high- and medium-ε_b cases, while a weak dependence of the ECE intensity on P_{abs} is obtained in the low-ε_b configuration. The ECE measurement indicates an increase in the

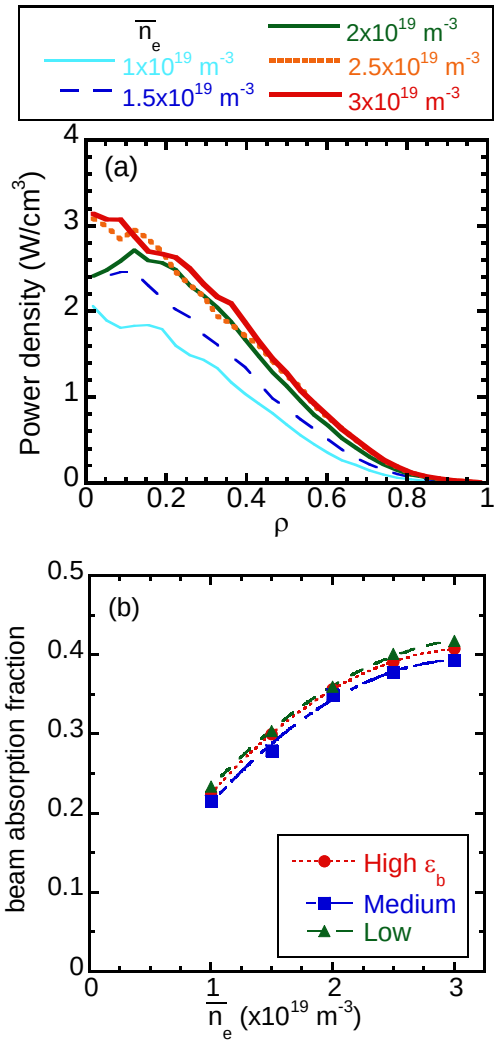

Fig. 3. (a) Radial profile of the beam absorption profile in the medium-ε_b configuration at the line-averaged electron density ($\bar{n}_e$) of 1, 1.5, 2, 2.5 and 3x10^{19} m^{-3}, and (b) beam absorption fraction as a function of line-averaged electron density in the high-, medium- and low-ε_b configurations.

electron temperature both in high- and medium-ε_b configurations. Although the ECE measurement does not calibrated absolutely, the configuration dependence of the stored energy plotted in Fig. 4 can be explained qualitatively in terms of the difference in the ion and electron temperatures.

Figure 6 shows the comparison of the experimental energy confinement time τ_E^{DIA} with the International Stellarator Scaling law ISS95 (τ_E^{ISS95}). The beam component of the stored energy is deduced from the Fokker-Planck analysis. It is less than 7 % under these conditions and is subtracted from the obtained stored energy. The enhancement factor of the energy confinement to the scaling ($H_{ISS95} = \tau_E^{DIA}/\tau_E^{ISS95}$) is about 1.8, 1.7 and 1.4 in the high, medium and low-ε_b configurations, respectively. These results indicate that the high and medium-ε_b configurations have better confinement characteristics than that for the low-ε_b configuration. From the viewpoint of the effective helical ripple ε_{eff}, we obtained a good plasma performance not only in the lowest ε_{eff} condition (i.e. medium-ε_b) but also in the higher-ε_{eff} configuration.

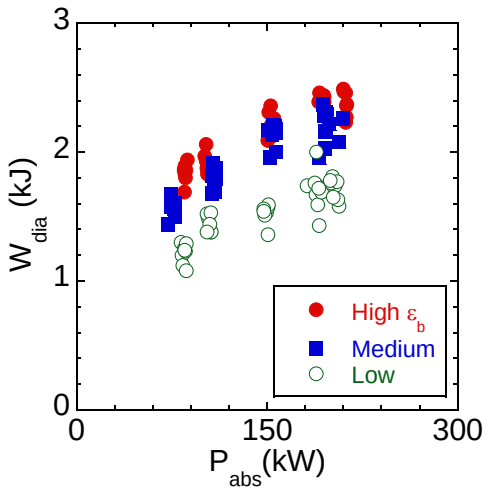

Fig. 4. Stored energy as a function of absorbed NBI power P_{abs} obtained in high-, medium- and low-ε_b configurations.

Here, we should describe the comparison of energy confinement between NBI and ECH plasmas of Heliotron J. In ECH plasmas, it has been found that the better enhancement factor of the energy confinement is obtained in the lowest ε_{eff} (medium-ε_b) condition and it decreases with increasing ε_{eff} [18-20]. In the NBI plasmas, since the bulk plasma is heated only by the slowing down of beam ions, the plasma performance should be strongly influenced by the fast ion confinement. From the previous study, a better confinement for the energetic particle has been found in the high-ε_b configuration. [13]; The decay time of the CX flux after the turning off of NBI has increased with increasing bumpiness. The numerical calculation shows the trapped particles survive longer in the high-ε_b configuration. Therefore, the high ion and electron temperature in the high-ε_b configuration shown in Figs 5(a) and 5(b) would be owing to the improvement in the energetic ion confinement. It may contribute to improve the energy confinement of the high-ε_b case.

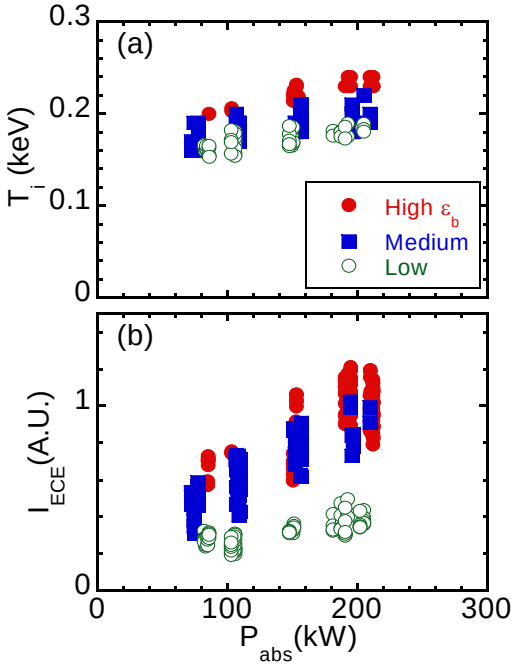

Fig. 5. (a) Bulk (deuterium) ion temperature and (b) ECE intensity as a function of P_{abs} in high-, medium- and low-ε_b configurations.

5. Summary

We investigate the global energy confinement

in the NBI plasmas of Heliotron J. The preferable energy confinement has been obtained not only in the lowest effective helical ripple condition but also in the configuration having good energetic ion confinement. The bumpiness control experiments have revealed the effectiveness of the control of bumpiness on the confinement both for the energetic particle and the bulk plasma. However, the relation between bumpiness or effective helical ripple and the anomalous transport is still an open question. Further experiments and analyses are needed to clarify the physical mechanism with attention to the plasma flow, rotation and radial electric field.

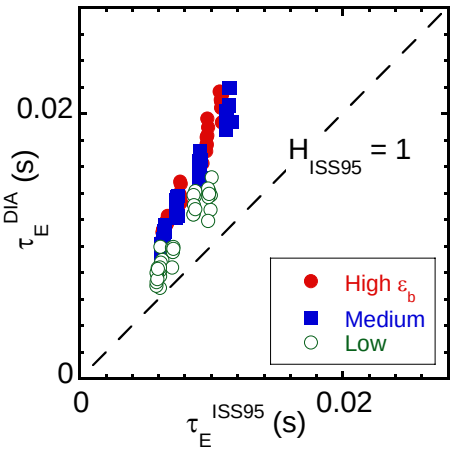

Fig. 6. Relationship between experimental energy confinement time and international empirical scaling law, ISS95, obtained in the NBI plasmas at the three bumpiness configurations.

Acknowledgements

The authors would like to express acknowledge to the Heliotron J staff for conducting the experiments. This work was supported by NIFS/NINS under the NIFS Collaborative Research Program (NIFS04KUHL005, NIFS04KUHL003, NIFS04KUHL006, NIFS05KUHL007, NIFS06KUHL007, NIFS06KUHL010, NIFS07KUHL011, NIFS07KUHL015 and NIFS08KUHL020) and under a project sponsored by the Formation of International Network for Scientific Collaborations. This work was partly supported by a Grant-in-Aid for Scientific Research from the Japan Society for the Promotion of Science No. 20686061.

References

[1] NÜHRENBERG, J. and ZILLE, R., Phys. Lett. A **129** (1988) 113.
[2] GARREN, D. A. and BOOZER, A. H., Phys. Fluids B **3** (1991) 2822.
[3] MOTOJIMA, O., et al., Nucl. Fusion **47** (2007) S668-S676.
[4] OBIKI, T., et al., IAEA-CN-56/C-1-2 (1066).
[5] OKAMURA, S., et al., Nucl. Fusion **45** (2005) 863–870.
[6] MURAKAMI, S., et al., Nucl. Fusion **42** (2002) L19–L22.
[7] YAMADA, H., et al., Plasma Phys. Control. Fusion **43** (2001) A55–A71.
[8] OKAMURA, S., et al 1999 Nucl. Fusion **39** (1999) 1337.
[9] SANO, F., et al., J. Plasma Fusion Res. SERIES **3** (2000) 26.
[10] OBIKI, T., et al., Nucl. Fusion **41** (2001) 833.
[11] WAKATANI, M., et al., Nucl. Fusion **40** (2000) 569.
[12] YOKOYAMA, M., et al., Nucl. Fusion **40** (2000) 261.
[13] KOBAYASHI, S., et al., IAEA-CN-116/EX/P4-41 (2004)..
[14] NEMOV, V. V., et al., Phys. Plasmas **6** (1999) 4622.
[15] WAKASA, A., et al., J. Plasma Fusion Res. **4** (2001) 408.
[16] MURAKAMI, S., et al., Trans. Fusion Tech. **27** (1995) 259.
[17] MCCOY, M.G., et al., Compt. Phys. Commu. **24** (1981) 37.
[18] SANO, F., et al., IAEA-CN-149/EX/5-5Ra (2006).
[19] MIZUUCHI, T., et al., Fusion Sci. Tech. **50** (2006) 352.
[20] MIZUUCHI, T., et al., Proc. International Congress on Plasma Physics 2008 (ICPP2008) O1-Y-6 (2008).